Time-space regulation of biomimetic vascularization in 3D printed skeletal muscles

Minxuan Jia[1,2,3,#] · Tingting Fan[1,2,3,#] · Tan Jia[2,3,4,#] · Xin Liu[1,2,3] · Heng Liu[1,5] · and Qi Gu[1,2,3 *]

Abstract

In the intricate skeletal muscle tissue, the symbiotic relationship between myotubes and their supporting vasculature is pivotal in delivering essential oxygen and nutrients. This study delves deep into the nuanced interplay between skeletal muscle cells and endothelial cells in the vascularization of muscle tissue. By harnessing the capabilities of 3D bioprinting and modeling, we employed a groundbreaking approach: co-constructing endothelial and muscle cells, followed by their subsequent differentiation. Our findings underscore the profound impact of the interaction dynamics between these two cell types. Notably, introducing endothelial cells during the advanced phases of muscle differentiation enhanced myotube assembly. It spurred the development of the vascular network, paving the way for the early stages of vascularized skeletal muscle. The methodology highlighted in this research illuminates the potential for creating large-scale, physiologically aligned skeletal muscle. Furthermore, it accentuates the need for deeper explorations into the delicate equilibrium and mutual interactions between muscle and endothelial cells. Guided by the multi-cell-type interaction model, we foresee promising pathways for crafting even more intricate tissues or organs.

Key Words: skeletal muscle · vascularization · 3D bioprinting · cell interaction

[#] Minxuan Jia, Tingting Fan, and Tan Jia contributed equally to this work.

Qi Gu
qgu@ioz.ac.cn

[1] State Key Laboratory of Membrane Biology, Institute of Zoology, Chinese Academy of Sciences, Chaoyang District, Beijing 100101, People's Republic of China

[2] Beijing Institute for Stem Cell and Regenerative Medicine, Chaoyang District, Beijing 100101, People's Republic of China

[3] University of Chinese Academy of Sciences, Huairou District, Beijing 100049, People's Republic of China

[4] State Key Laboratory of Stem Cell and Reproductive Biology, Institute of Zoology, Chinese Academy of Sciences, Chaoyang District, Beijing 100101, People's Republic of China

[5] Department of Orthopaedics, Beijing Jishuitan Hospital, Capital Medical University, Beijing 100035, People's Republic of China

Introduction

In skeletal muscle tissue, 85% are multinucleated myotubes, with the remaining 15% attributed to the nervous system, vasculature, and connective tissue. [1-3] Capillaries distributed around muscle bundles serve a dual purpose during skeletal muscle development. They are essential for supplying oxygen and nutrients and are pivotal in promoting skeletal muscle tissue generation and repair. [4-6] Following muscle injury, endothelial cells are activated by biological and mechanical cues, forming new vascular networks. [7] The interplay between the vascular network and muscle fibers is intimately linked, greatly influencing the injury repair process. [8] Notably, when a skeletal muscle defect exceeds 20%, it results in volumetric muscle defects. [9] Currently, the primary clinical treatment for these defects is autologous muscle transplantation; however, this approach often sees a high failure rate. [10,11] With the advent of tissue engineering, avenues for clinical treatments include 2D inoculation, 3D replication, and 3D printing technology. [11] The partial functionalization and cell orientation of skeletal muscle have been realized, and phased progress has been made in animal experiments. 3D printing has shown early success in the construction of vascularized skeletal muscle. [12]

Skeletal muscle is rich in vasculature, with each myotube intricately surrounded by a capillary network. [13] To recreate skeletal muscle structures where blood vessels envelop myotubes, interventional engineering methods are paramount. Understanding the vascular network formation in injured skeletal muscle necessitates a deep dive into the interactions between capillaries and myotubes. Owing to their delicate structure and intimate association, [8] constructing engineered vascularized skeletal muscle becomes essential to accurately assess the interplay between skeletal muscle myotubes and vascular endothelial cells. [14] In a biomimetic sense, vascular network development happens synchronously with skeletal muscle tissue differentiation *in vivo* [7]. Thus, determining the optimal timing for vascularizing skeletal muscle tissue *in vitro*, grasping the temporal and spatial dynamics of multi-cell co-culture, and crafting intricately structured vascularized skeletal muscle tissue is crucial.

A refined methodology exists for *in vitro* skeletal muscle construction, setting the stage for muscle vascularization. 3D printing was used to construct mature and oriented skeletal muscle, which can recover skeletal muscle function by 82%. [15] Fan et al used 3D bioprinting to construct skeletal muscle tissue and found that spatial constraints play an important role in the orientation differentiation of skeletal muscle. [16] However, innovating new tissue engineering techniques for crafting vascularized skeletal muscle suitable for in vivo transplantation and functional recovery is indispensable. Regarding cell orientation, the aligned microstructure can facilitate cellular cultivation and tissue transplantation. [17] Sequential modeling allows for tissue investigation in distinct tubes, emphasizing muscle-vascular interactions. [8] The mold can integrate cells within 3D hydrogels by co-culturing multiple cells, forming muscle bundles with vascular networks and motor neurons. [18]

Significant advancements have been made in recent years in the realm of tissue engineering for the in vitro construction and animal transplantation of vascularized skeletal muscle. For the construction of large-scale vascularized skeletal muscle, 3D sub-liquid coaxial printing was employed to encapsulate muscle bundles within a vascular network structure. This approach found that up to 85% of the functional damage of volumetric muscle defects could be restored post-transplantation. [12] While this strategy effectively upscales tissue construction, the 3D printing method has limitations. In such systems, tailoring the timing for each cell based on its unique properties remains a hurdle. However, there are still many challenges: (1) develop and refine methods for constructing functional biomimetic vasculature and skeletal muscle; (2) establish a multicellular co-culturing system that supports self-assembly and differentiation capabilities; (3) optimize the timing of bioactive signals and nutrient supply to target cell types in a multicellular system. Developing new tissue engineering methods to construct vascularized skeletal muscle is critical.

This study examined multi-cell co-cultures temporal and spatial dynamics in skeletal muscle tissue, aiming to construct vascularized muscle tissue with intricate structures. Results highlighted the effectiveness of the 3D demolding method and the influence of vascular network formation on muscle differentiation. Ultimately, 3D printing and precise timing adjustments can produce vascularized skeletal muscles with mature myotubes, setting the stage for future research on advanced muscle structures and multicellular systems.

Materials and methods

Cell culture

The mouse myoblast cell line C2C12 was obtained from the Shanghai Cell Bank of the Chinese Academy of Sciences. The C2C12 was cultured in proliferation medium (PM) consisting of Dulbecco's modified Eagle's medium (DMEM) / high glucose (C11965500BT, Gibco), fetal bovine serum (FBS, 10%; 10099-141 C, Gibco), and penicillin / streptomycin (PS) (1%; C11965500BT, Gibco) for two days within 15 generations under 5%CO_2 at 37℃. The human umbilical vein endothelial cell (HUVEC) and RFP-HUVEC were obtained from Prof. Lijian Hui's group. The HUVEC and RFP-HUVEC were cultured on gelatin (0.1% w / v, G1890, Sigma) - coated 10 cm cell-culture petri dish in Endothelial cell growth medium - 2 (EGM - 2; CC3162, Lonza) for three days within 14 generations under 5%CO_2 at 37°C.

Bioink preparation

DMEM dissolved gelatin (G1890, Sigma) at 37℃ 1 hour. Fibrinogen (F8630, Sigma) was dissolved in sanitary water (BL100310) at 37℃ for 2 hours. Thrombin (T4648-1KU, Sigma) was dissolved in PBS. The C2C12 cell-laden bioink consisted of fibrinogen (20 mg/mL) and 5% (w/v) gelatin at a concentration of 1×10^7 cells / mL. The HUVEC was encapsulated in the mix of fibrinogen (10 ~ 20 mg / mL) and thrombin (2 unit/mg) at a $5\times10^6 \sim 1\times10^7$ Cells / mL concentration. The HUVEC-containing cell hydrogel (fibrinogen / gelatin) mixture (HFG) consisted of fibrinogen (10 ~ 20 mg / mL), 5% (w/v) gelatin, and thrombin (2 unit/mg) at a $5\times10^6 \sim 1\times10^7$ cells / mL concentration.

3D printing of anchor and polydimethylsiloxane (PDMS) model

Weigh the printed PDMS (SE1700, DOWSIL) stock solution 5 g and curing agent (stock solution: curing agent = 10:1), mix and defoam, put it in the printing cartridge, and defoaming, install it on the 3D printer (Bio-Architect®-WS). Open the Bio Architect software, import the model drawn in Solidworks into the printer, and set the printing speed, thickness, and number of layers. The printing pressure was maintained from 0.25 MPa to 0.35 MPa, and the printing scaffold was started after the filament was smoothly tested. The struts constructed using a light-curing printer (Stratasys Object260 Connex3) were fixed to both ends of the PDMS frame and cross-linked at 60°C for four hours. The scaffolds were removed and sterilized.

Demolding model of the PDMS model was printed by Ultimaker. PDMS (DKN1841100) stock solution 5 g and curing agent (stock solution: curing agent = 10:1), mix and defoam. Added PDMS in the demolding model, degasser the mold in a vacuum for 30 min, and then the PDMS mold was kept at 40℃ for 24 h. The PDMS mold was removed and sterilized with ethylene oxide. Modify the groove width parameter of demolding model according to the fascicle width (800 μm~1200μm).

3D bioprinting of muscle constructs

The SIA PRO printer developed by the Shenyang Institute of Automation, Chinese Academy of Sciences, was used for 3D bioprinting. C2C12 cell-laden bio-ink was prepared and pre-cooled at 4°C for 10 min in a special SIA Bioprinter barrel. Install the barrel to the specified position, adjust the temperature of the platform to 6℃, and control the nozzle's and the needle's temperature to 18℃ ~ 25℃ to ensure that the filament state is maintained in the gel state. Calibrate the nozzle, calibrate the base plate, set the end position of printing as the origin of printing, and save and download parameters. Then, the model drawn in

advance was imported, the silk condition was tested, and the muscle bundle was printed.

In vitro culture of muscle bundles

The anchor was inserted into both ends of the printed construction and added thrombin (20 unit/mg) was covered around the hydrogel, cross-linked at 25℃ 45 min, and then 37℃, 10 min. Put muscle bundles into 6-well plates to culture with PM [2 mg/mL 6-Aminocaproic acid (6-AA; A2504-25G, Sigma)] for one day. Then the medium to differentiation medium (DM), which consisted of DMEM, 2% horse serum (HS; 26050088, Gibico) 1%PS, 2 mg/mL 6-AA, and 1 μmol/mL Insulin (I6634, Sigma), and the medium was changed daily.

Constructed of vascularized muscle bundles

For the adhesion monolayer cell formation method, the one-day differentiated (DM 1) muscle bundle was placed in the PDMS mold, and HUVEC cell suspension at a density of 5×10^6 cells / mL was added to the groove until the muscle bundle was removed entirely at 37℃ for 30 minutes. The muscle bundle was then turned over, and the cell suspension was replenished until completely unwashed at 37 °C for 30 min. The muscle bundles adhered to RFP-HUVEC were then placed in six-well plates, the differentiation medium 50% DM + 50% EGM2 was added, and the medium was changed daily. HFG wrapping method: The DM 1, DM 4, or DM 7 muscle bundles were placed on the "3 - in - 1" mold, and HFG with HUVEC density of $5\times10^6 \sim 1\times10^7$ cells / mL was added to the groove. The top cover was installed and placed at 37℃ for 6 min. The muscle bundles were removed in 6-well plates and co-culture for six days, called DM1+6, DM4+6, and DM7+6 groups. The medium was changed daily.

Rheological tests

The test samples were 5% gelatin - 2% fibrinogen, 3% gelatin - 2% fibrinogen, and 5% gelatin. 3% gelatin, using a rotor of pp - 25mm. The shear thinning test conditions were as follows: test temperature 8℃, test strain 1%, shear rate 0.001 ~ 100 1/s, and 8℃ heat preservation for 5 min to start the test. The temperature scan test conditions were as follows: the test temperature range was 4 to 40 °C, the test strain was 1%, the shear rate was 1%, and the test was started by holding at 40 °C for 5 min. The frequency scan test conditions were as follows: test temperature 8°C, test strain 1%, shear frequency 0.01 to 10 Hz, and start after holding at 8 °C for 5 min. The test conditions for alternating strain changes were as follows: the test temperature was 8 °C, the strain change was 0.5% for 100 s, and then the change was 500% for 100 s, alternating for 6 cycles, and the experiment was started after 5 min of insulation at 8 °C.

Cell viability tests

An appropriate volume of staining solution with the concentration of 0.5 μL / mL calcein, 2 μL / mL ethidium bromide dimer, and Hoechst (1:1000) was added to the sample so that it did not pass the model entirely. The staining condition was 37℃ in the dark for 30 min. The staining solution was discarded, washed once with PBS, and the medium was added and observed under a dragonfly microscope. The number of viable cells (green) versus dead cells (red) was counted using image j, and cell viability was calculated by dividing the number of viable cells by the total number of cells (n = 3).

Histologic and Immunofluorescence Staining

Samples were fixed using 4%PFA for 24h and washed thrice in PBS to prepare staining. Routinely treated and embedded in paraffin. Place transverse sections on salinized slides for immunohistochemistry by CD31(ab28364). The other samples were fixed using 4%PFA for 24h and washed thrice in PBS to prepare staining. The samples were thoroughly immersed in 1% (w / v) Triton dissolved in PBS with permeable membrane solution, placed on a shaker, incubated for 2 h at 25°C, and washed three times with PBS. Samples were thoroughly soaked by adding 5% (w / v) BSA solution and placed on a shaker overnight at 4°C. MHC antibody was diluted 1:200 in the blocking solution, CD31 antibody was diluted 1:200, and VE - Cad antibody was diluted 1:200 in the blocking solution. DAPI was diluted 1:1000 on a shaker overnight at 4 °C. Then PBST (10 mL = 10 mL PBS + 10 μL 1 / 1000 Tween - 20 + 10 μL Triton X - 100) was added 3 times, 30 min each time. Secondary

antibodies were diluted with PBST at 1:500 and incubated for 2h at room temperature in the dark. They were placed on a shaker at room temperature and washed thrice with PBST for 30 minutes each time. Staining was observed with a confocal microscope or live cell workstation.

Quantitative reverse transcription polymerase chain reaction (RT - qPCR) analyses

The expression levels of mouse myogenic and vascularized genes in vascularized skeletal muscle were assessed by two-step RT-qPCR. When the vascularized skeletal muscle was differentiated and cultured to Days 7, 10, and 13, the samples were removed, and 800 μL of Trizol was added. RNA was extracted using glycogen (Thermo Fisher Scientific, R0551) using standard methods, and RNA (1 μg) was reverse transcribed into cDNA using PrimeScript™RT Master Mix (TaKaRa, RR036A); they were then diluted with RNase-free water. Expression levels of myogenic differentiation genes (mMyoD1, mMyf5, mMyoG, mMyh1, mMyh2, mMyh4 and mMyh7) mixed with vascularization genes (CD31, CD34, CD144 and vWF) were analyzed using Hieff®qPCR SYBR Green Master (No Rox) (Yeasen, 11201ES03). GAPDH is used for internal standardization. Primers for RTqPCR in this study are listed in Table 1 (see supplementary information). Data analysis followed the following formula, where cDNA cycle threshold (CT) values were derived from real-time PCR software, and CT values were derived from the average CT values of 3 samples:

(a) d CT (sample, gene) = CT (sample, gene) – Average (CT (sample, GAPDH))

(b) dd CT (sample, gene) = d CT (sample, gene)– Average ((d CT (control, gene)))

© Foldchange = 2 ^ − dd CT (sample, gene).

Statistical analyses

All data are presented as mean ± standard deviation. The t-test was used for statistical significance. GraphPad Prism 8 (Sy stat software) was used for statistical analysis. Statistical significance said as follows: * $p < 0.05$, ** $p < 0.01$, *** $p < 0.001$, **** $p < 0.0001$.

Results

Fabrication and characterization of the muscle bundle

In this study, we examined the rheological analysis of a hydrogel system comprised of gelatin + fibrinogen (referred to as Gel - Fib hydrogel). Due to gelatin's thermosensitive nature, the phase transition point of 5%gelatin + 2%fibrinogen was identified at 22℃ (Figure 1A). It was found that the viscosity of the materials used in the four groups of experiments decreases with the increase of shear rate, which has the property of shear thinning (Figure 1B), so the damage of cells will reduce when the printing needle extracts the material. [19] In addition, the Gel + Fib hydrogel group had strong mechanical properties, which could stack multi-layer hydrogel (Figure S1A). Then, the ink was maintained in a printable state extruded from the needle by adjusting the temperature (Figure 1C). Subsequently, the form of the hydrogel during and after extrusion by adjusting the rapid change of strain. It was demonstrated that the state of the four materials could be maintained stable in the change cycle, indicating that gelatin and Gel - Fib could quickly recover after extrusion and were suitable for 3D printing (Figure S1B). These results suggest that the Gel - Fib hydrogel has strong printing stability accompanied by characteristics of shear thinning, self-healing, and high modulus.

Skeletal muscle bundles were constructed according to the 3D bioprinting method. In this study, an H-shaped structure was erected by 3D bioprinting.[16] Then, scaffolds were installed at both ends to maintain the unidirectional force required for skeletal muscle differentiation (Figure 1D i). Gel - Fib hydrogel was used as cell-loaded printing ink to print muscle bundles with 14 mm × 1 mm × 2 mm on the slides (Figure 1D ii ~ iv). After printing, the scaffolds constructed by 3D printing in advance were fixed to both ends of the printed muscle bundles and then cross-linked after dropping the thrombin. The width of the muscle bundle changed significantly at the beginning of culture. (Figure S2). Live/dead staining

assay presented the number of live cells was even more with 90%cell viability (Figure 1F) when proliferated for one day to maintain the C2C12 adhere to the hydrogel stably (Figure 1H). It is proved that constructing muscle bundles by 3D bioprinting has less effect on the C2C12 and contraction during the culture of muscle bundles.

Myoblasts format to multinucleated myotubes through migration, orientation, and membrane fusion. [1] Staining of the cytoskeleton showed that C2C12 showed exposure on the 4th day of differentiation and was more evident on the seventh day of differentiation and culture (Figure S3A). The orientation distribution ratio of cells showed that the orientation of cells

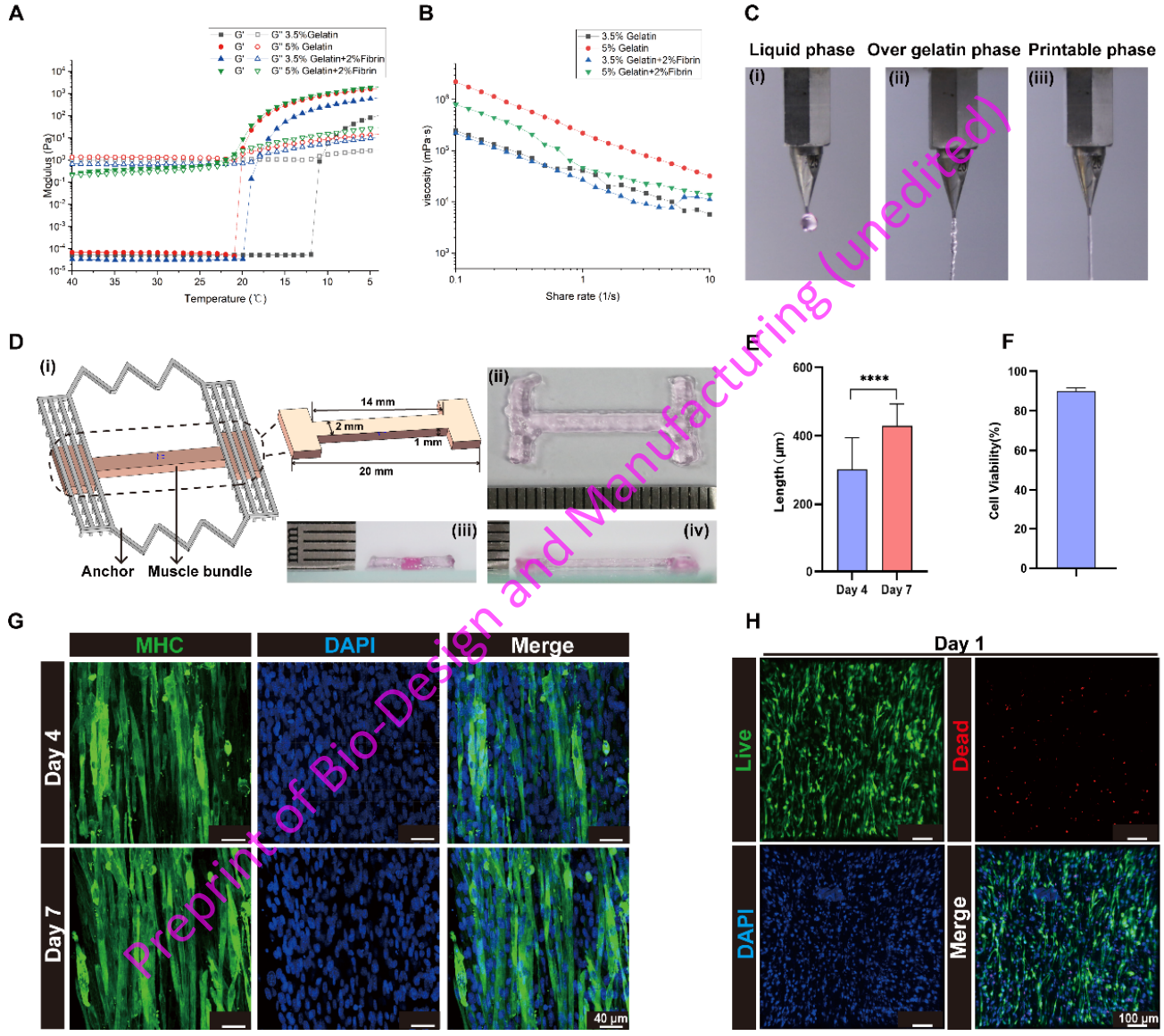

Figure 1. Construction of skeletal muscle by 3D printing. (A) Temperature across curves of gelation and gelation-fibrinogen (40°C to 4°C, 1 Hz, strain 1%). (B) The shear rate ranges from 0.1 to 10 1 / s across curves of gelation or fibrinogen (strain 1%, 8°C). (C) Extrusion of 3.5%gelation＋2%fibrinogen shows the liquid, over-gelation, and printable phases at different temperatures. (D) The schematic illustrations and optical images of construction.(i) The schematic illustrations of muscle bundle and PDMS anchor; (ii ~ iv) Aerial view, left view, and front view of printed constructio©(E) The length of the muscle tube was calculated on day four and day 7. (**** $p < 0.0001$, n = 3). (F) Myoblast cell viability after 1-day proliferation (n = 3). (G) Immunolabeling for myosin heavy chain (MHC, green) with Hoechst counterstain is used to assess the degree of myogenic differentiation on day four and day 7. (H) The live (green) and dead (red) staining after 1-day proliferation. Scale bar: (G) 40 μm; (H) 100 μm.

increased significantly on the 7th day of fasciculation (Figure S3B). Therefore, it was found that myoblasts are gradually oriented and arranged following the process of differentiation and culture. The formation of myotubes in muscle bundles was observed by immunofluorescence staining. It was demonstrated that shorter primary myotubes were formed on the fourth day and that myotubes continued to fuse to form longer secondary myotubes on the seventh day during the differentiation process of muscle fasciculus (Figure 1G, Video 1). The myotubes length measured by image J showed a significant increase in myotubes length on day 7 (Figure 1E). It was found that myoblasts fuse to longer multinucleated myotubes during differentiation of muscle bundles.

HUVEC was wrapped outside the muscle bundle to construct vascularized skeletal muscle

The vascular network was constructed as thin as possible to build a more bionic vascularized skeletal muscle and satisfy the 200 μm nutrient-delivery restriction. [20] We designed two construction strategies to construct the vascular network: Figure 2A i shows monolayer HUVEC adhering outside the muscle bundle during differentiation, and Figure 2A ii shows the HFG wrapping around the muscle bundles at stages of differentiation.

The HUVEC can achieved equably outside the muscle bundle on the first day of differentiation (Figure S4A). However, HUVEC gradually falls off during differentiation and culture, and the cell density of HUVEC can not satisfy the formation of a vascular network on the fourth day (Figure 2B). Then, adhere HUVEC outside the muscle bundles to differentiate for three days. It was found that a high density of HUVEC could conform to the outside of the muscle bundles, which differentiated to 1 ~ 3 days (DM 1~3) (Figure S4A). HUVEC were gradually shed from muscle bundles in the three groups during three days of continuous culture (Figure S4B). The results showed that the change in muscle bundle volume affected the adhesion of HUVEC. Therefore, the adhesion methods that adhere HUVEC outside the muscle bundle could not achieve the construction of vascularized skeletal muscle.

Wrap HFG was used to construct vascularized skeletal muscle, and the hydrogel provided a growth space for HUVEC to maintain the long-term culture outside the Fascicle. Adherent HUVEC could not achieve the differentiation of myotubes outside the muscle bundle (Figure 2C). Wrapping HFG outside the muscle

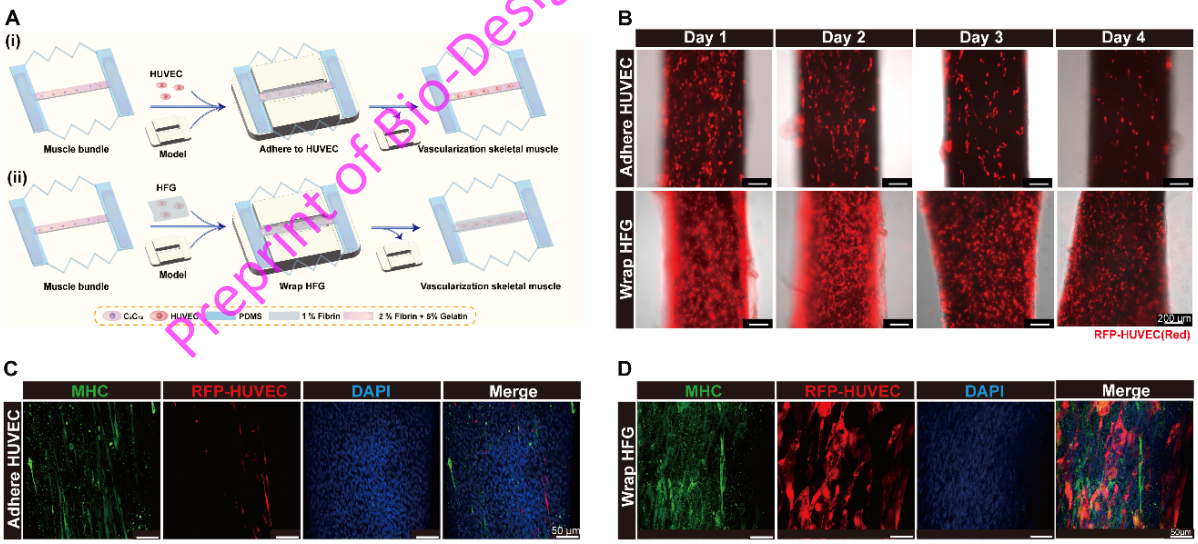

Figure 2. Evaluation of the way to construct vascularized skeletal muscle. (A) Schematic illustration of adhering HUVEC to muscle bundle (i) and wrapping the HFG outside the muscle bundle by 3D printing (ii). (B) Immunolabeling for MHC (green) with Hoechstis and RFP - HUVEC was used to assess the degree of myogenic differentiation and self-assembling of HUVEC on day 7. (C) HUVEC (red) adhesion was observed continuously with a microscopy image of the muscle bundle for four days. (D) The state of HUVEC (red) maintenance of muscle fiber was observed continuously with microscopy images for four days. Scale bar: (B) 200 μm; (C ~ D) 50 μm.

bundle showed that HUVEC can adhere around the muscle bundle for four days and begin to extend (Figure 2B). It was indicated that the cell viability of HUVEC was more than 90% after one day of culturing into 1% and 2% fibrin for 3D culture (Figure S5). HUVEC encapsulation was evident on the outside of the bundle after seven days of differentiation, and myotubes appeared within the entire bundle (Figure. 2D). Therefore, this method can initially achieve the construction of vascular skeletal muscle with blood vessels and multinucleated myotubes.

PDMS release mold used to wrap hydrogel outside the muscle bundle called a “three-in-one” mold (Figure 3A). The operation of PDMS to wrap the hydrogel into a muscle bundle is more suitable due to the soft

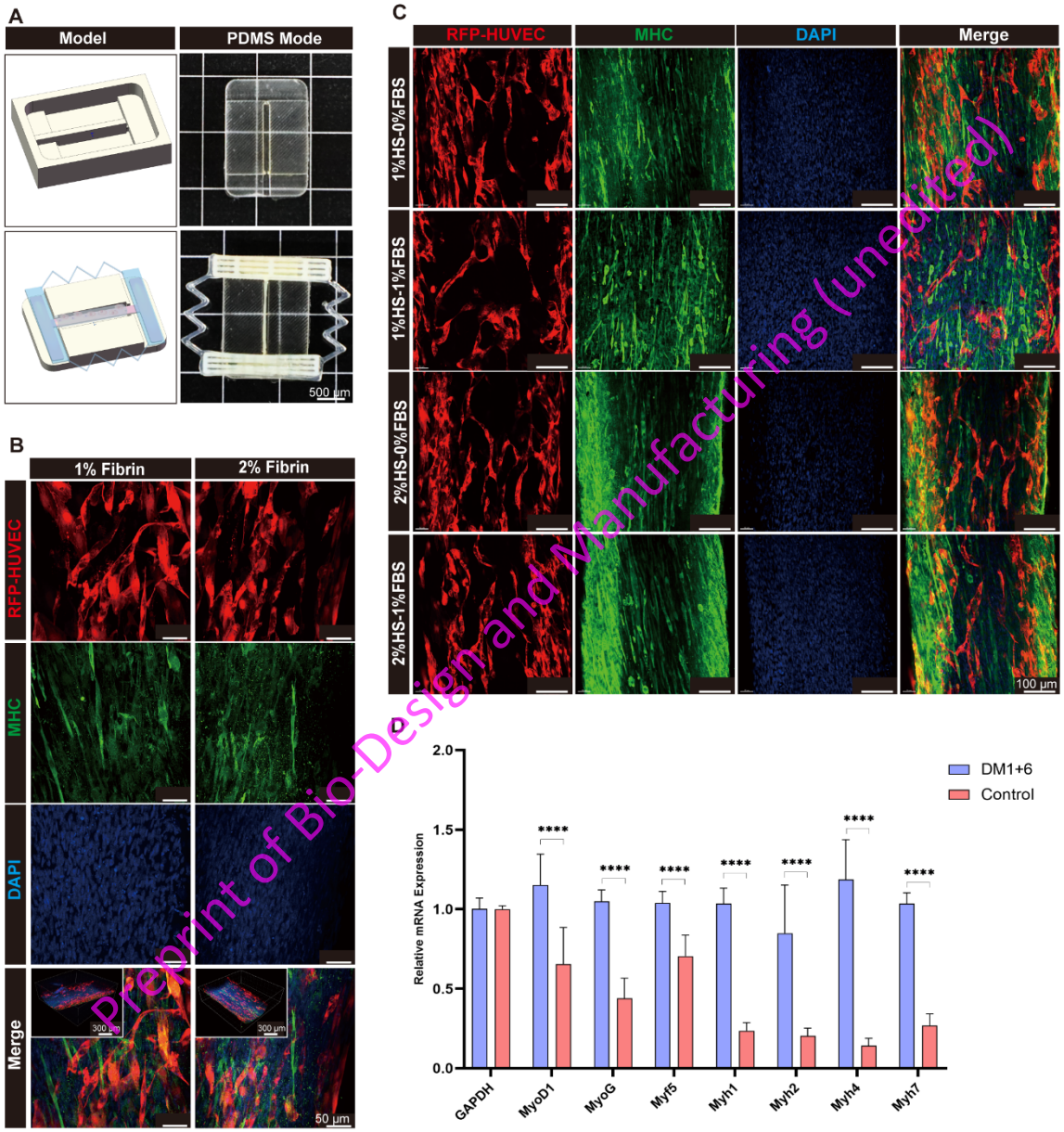

Figure 3. Optimization of constructing vascularized skeletal muscle to culture. (A) Demolding model and working illustration of PDMS mold. (B) Using four kinds of medium (HS - FBS), culture 1-day differentiation muscle bundles which wrapped 1% HFG, the fusion of myotubes (MHC, green), and self-assembling of HUVEC (red) was observed. HUVEC (red), MHC (green), DAPI (blue). (C) The DM 1 muscle bundles were wrapped with 1% and 2% fibrin and then cultured to day 7 (DM1+6). HUVEC (red), MHC (green), DAPI (blue). (D) The expression levels of C2C12 differentiated myogenic marker genes (MyoD1, MyoG, Myf5, Myh1, Myh2, Myh4, and Myh7) in vascularized skeletal muscle were analyzed by quantitative qPCR in DM1 + 6 and DM7 groups. (**** $p < 0.0001$, n = 3). Scale bar: (A) 500 μm (B) 50 μm, 300 μm; (C) 100 μm.

material of PDMS [21], which can be easily removed from the mold because PDMS has strong hydrophobicity and less adhesion to fibrin.[22]

HUVEC mixed 2% fibrin coated outside the DM 1 muscle bundle showed poor extension on the 3rd day (Figure S6). It was observed that the vascularization was not obvious, and almost no myotubes formed in 7 days. HUVEC showed an evident stretching phenomenon on the 3rd day in the 1% fibrin group; vascularization could be seen in 7 days of differentiation, and primary myotubes could be seen inside the muscle bundles (Figure. 3B).

We screened the co-culture medium to form the vascular network and dense secondary myotubes to achieve the co-differentiation of HUVEC and C2C12 in vascularized skeletal muscle. It was found that HUVEC has high cell viability and can extend after culturing three days with different concentrations of HS and FBS (Figure S7). Next, we used the same medium formulation for differentiated vascularized

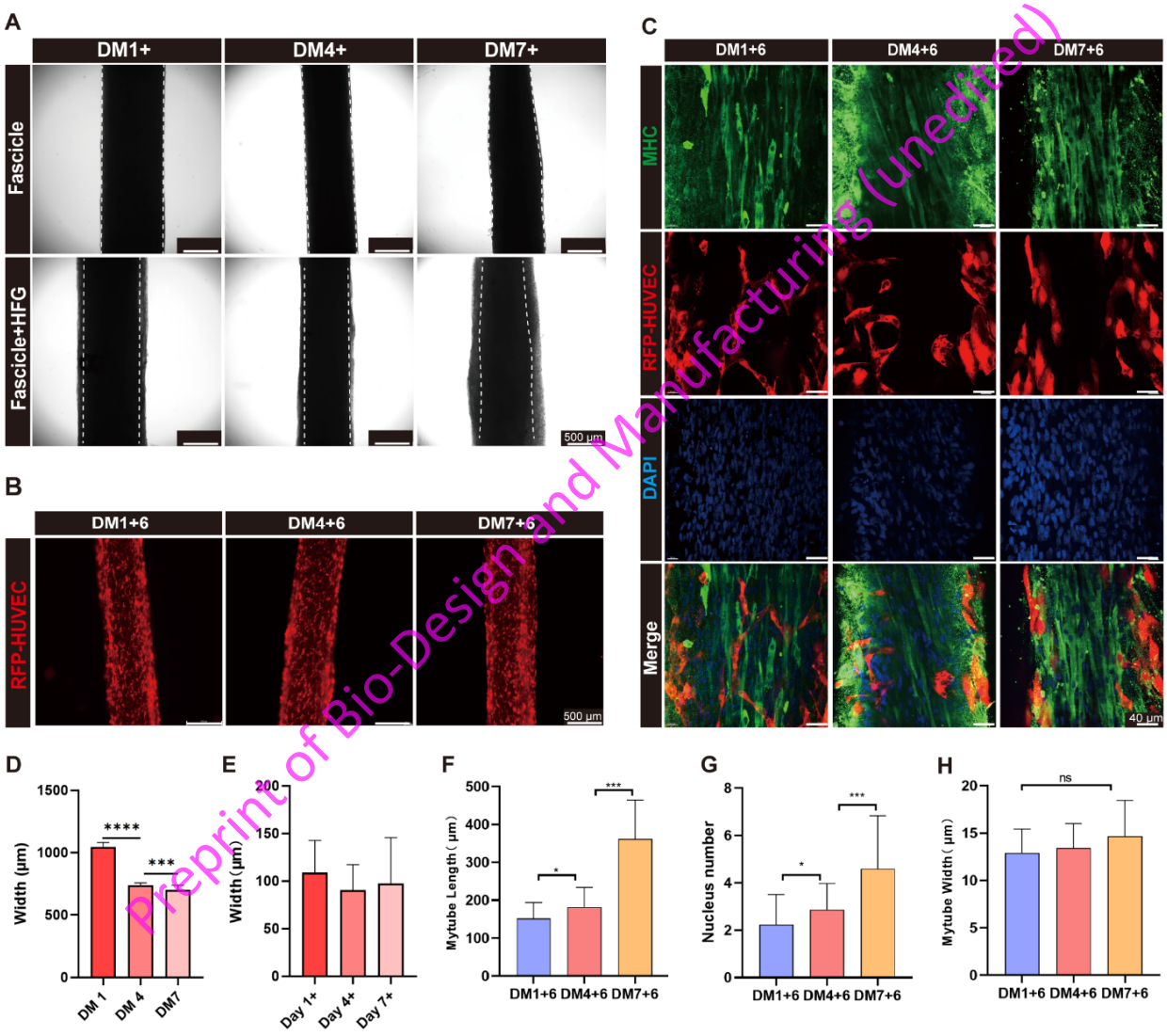

Figure 4. The vascularized skeletal muscle was constructed by wrapping HFG to muscle bundles at different days of differentiation. (A) Light microscopic observation of differentiated 1, 4, and 7 days muscle bundles were wrapped HFG. (B) Fluorescence microscope observation of differentiated 1, 4, and 7-day muscle bundles with HUVEC (red) was cultured for six days. (C) Fusion of myotubes (MHC, green) and self-assembling of HUVEC (red) were observed when wrapped HFG to differentiate different time muscle bundles. (D) The width of muscle bundles was quantitated in DM1, 4 and 7. (E) The thickness of HFG outside the muscle bundles was quantitated. (F ~ H) Quantitative statistics of myotubes length, width, and nucleus of DM1 + 6, DM4 + 6, and DM7 + 6. (* $p < 0.5$, *** $p < 0.001$, **** $p < 0.001$ n = 3) Scale bar: (A) 500 μm; (B) 500 μm; (C) 40 μm.

skeletal muscle tissue cultures. HUVEC self-assembly and vascularization are more pronounced at 1% FBS concentrations in the DM1+6 group (Figure 3C). Multinucleated myotubes appeared when HS concentration was increased to 2 %.

The myogenic differentiation of vascularized and non-vascularized muscle bundles in the same medium (2% HS - 1% FBS) was analyzed by RT-QPCR. The mRNA expression levels of MyoD1, MyoG, Myf5, Myh1, Myh2, Myh4, and Myh7 in the vascularized muscle bundles (DM1+6) were higher than those in the non-vascularized muscle bundles (Figure 3D). This indicates that the construction of a vascular network can promote the differentiation and maturation of myotubes.

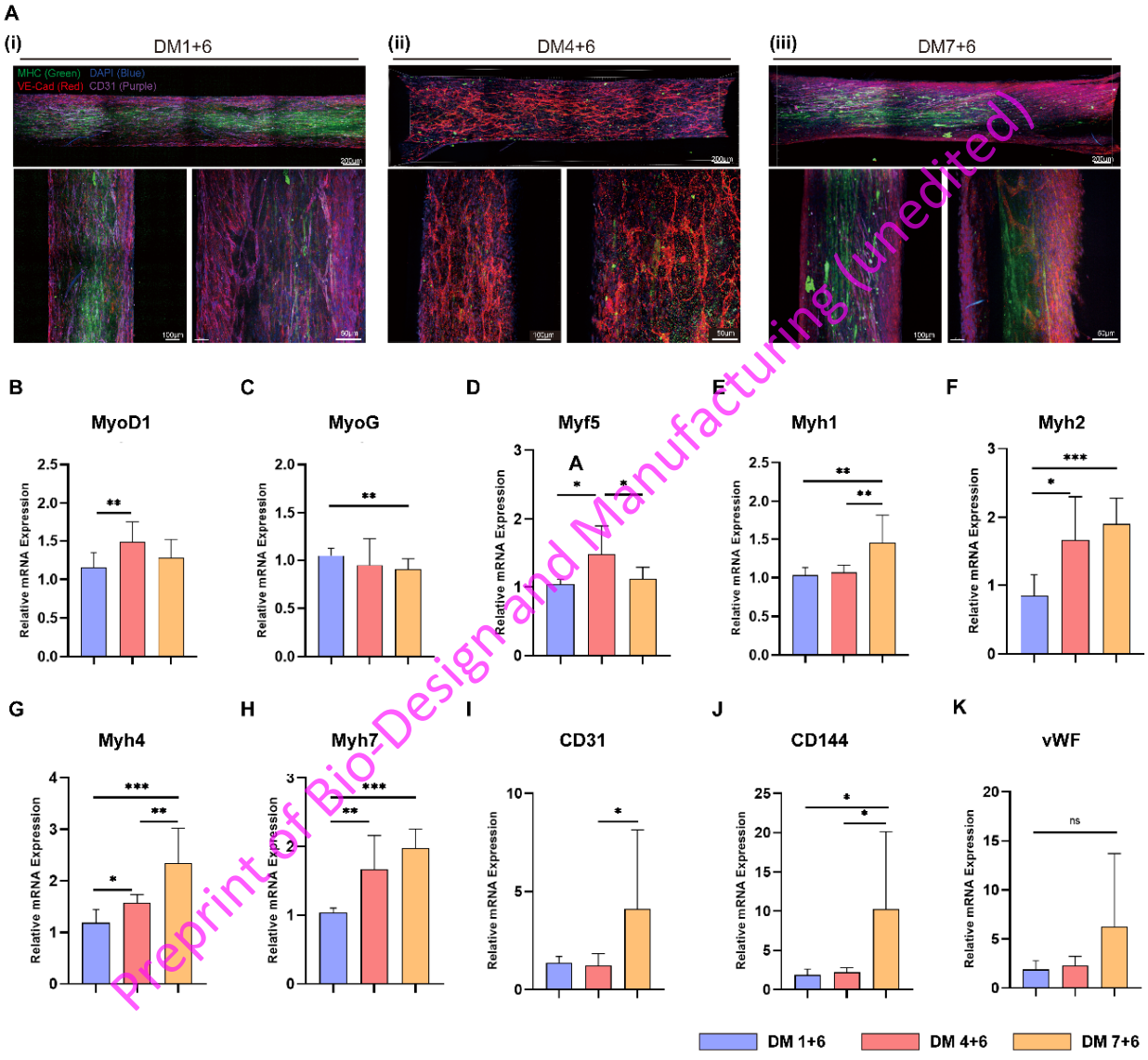

Figure 5. Differentiation of myotubes and blood vessel formation in vascularized skeletal muscle. (A) HFG was outsourced to the muscle bundles 1, 4, and 7 days after differentiation, and then vascularization construction was performed for six days to observe the differentiation of muscle tubes and blood vessels. (i ~ iii) The vascularization of DM1 + 6, DM4 + 6, and DM7 + 6 in the following three groups was depicted: CD31 (purple), VE - Cad (VE-cadherin, red), MHC (heavy chain myosin, green), DAPI (nucleus, blue). (B ~ H) The expression levels of C2C12 differentiated myogenic marker genes (MyoD1, MyoG, Myf5, Myh1, Myh2, Myh4, and Myh7) in vascularized skeletal muscle were analyzed by quantitative qPCR in DM1 + 6, DM4 + 6, and DM7 + 6 groups. (* $p < 0.05$, ** $p < 0.01$, *** $p < 0.001$, n = 3). (I ~ K) The expression levels of HUVEC vascularization marker genes (CD31, CD144, vWF) in vascularized skeletal muscle were analyzed by quantitative qPCR in DM1 + 6, DM4 + 6, and DM7 + 6 groups. (* $p < 0.05$, n = 3) Scale bar: 200 μm (top), 50 μm (below)

The time of vascular network construction affects myotube differentiation

To explore the effect of differences in vascularization time on vascular and skeletal muscle, using the "three-in - -one" mold to wrap HFG outside the muscle bundles on the 1st and 4th for 7th-day differentiation (Figure 4A). Hydrogel with thickness of about 100 μm could be surrounded outside the muscle bundles on different days of differentiation (Figure 4E) and the width of the muscle bundle was decreased during differentiation (Figure 4D). The DM1, DM4, and DM7 muscle bundles encapsulated with HFG differentiated to three days. HUVEC gradually extended, and almost no cells were shed during the culture period (Figure S8). HUVEC showed an apparent extension phenomenon and uniform distribution on the 6th day of differentiation, achieving a long-term culture of HUVEC (Figure 4B).

Next, to explore the effect of vascular network construction time on myotubes differentiation, we verified the effect of vascular network construction by muscle bundles differentiated into different stages and found that myotubes and vascular networks were formed in all three groups (Figure 4C, Video 2). The myotubes were shorter in the DM1 + 6 group, and most of them were primary myotubes with two nuclei. In the DM4 + 6 group, longer myotubes with three nuclei (about 200 μm) began to appear. However, in the DM7 + 6 group, the myotubes grew to about 350 μm, with about five nuclei in a single myotubes and longer secondary myotubes (Figure 4 G~H). There was no significant difference in the width of the myotubes among the three groups (Figure 4 H). The appearance of multinucleated myotubes is a vital indicator to show thee mature of myoblasts. [23] According to the above statistics, the length, and the number of nuclei in the DM7 + 6 group were the highest. Therefore, on the 7th day of muscle bundle differentiation, HUVEC was added to construct vascularized skeletal muscle, longer myotubes could formed, and the muscle bundle was more mature.

The expression of CD31 and VE - Cad was observed in DM1 + 6, DM4 + 6, and DM7 + 6 groups, indicating a tight junction between HUVECs and endothelialization. [24] Observation of the self-assembly state of HUVEC showed that there were tube network connections and myotubes formation (Figure 5A, Figure S9, Video 3). To verify the degree of myogenic differentiation and vascularization at the molecular level, the differentiation genes MyoD1, MyoG, Myf5, Myh1, Myh2, Myh4, and Myh7 of

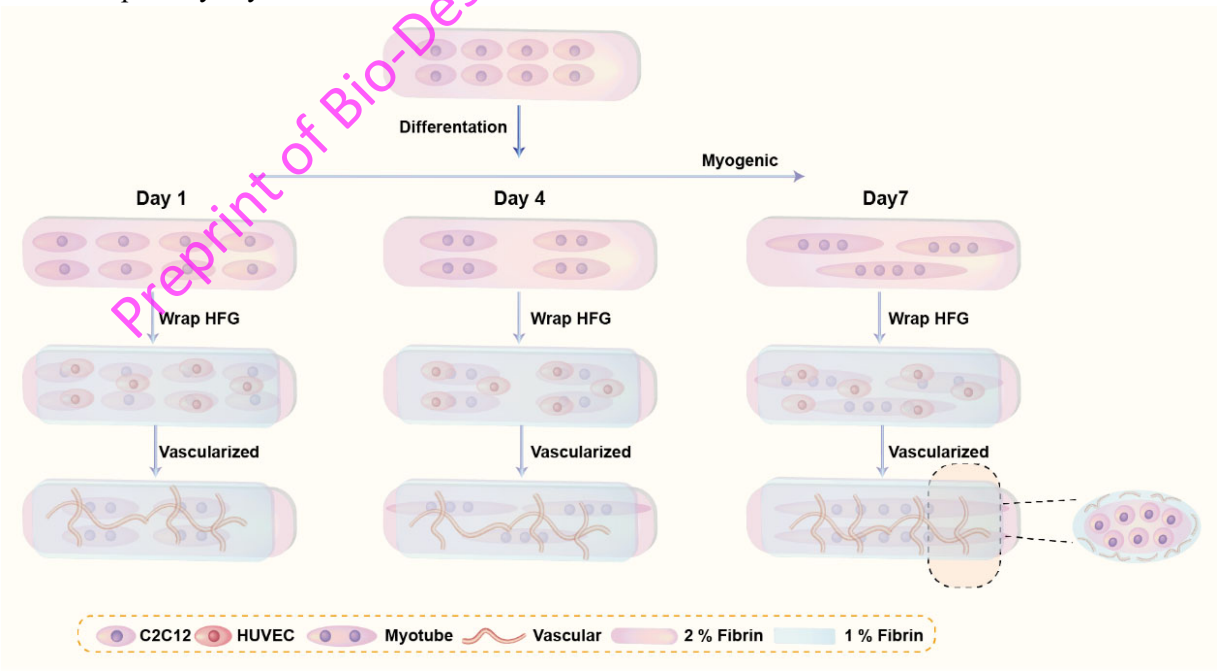

Figure 6. The differentiation process of vascularized skeletal muscle. This schematic shows that the formation of vascular networks at different stages of muscle bundle differentiation ultimately affects the maturity of vascularized skeletal muscle.

C2C12 cells were detected by RT-qPCR (Figure 5B ~ H). Compared with the DM1 + 6 group, the expression of MyoD1 in the DM4 + 6 group was higher, indicating that most of the myoblasts in the DM4 + 6 group were in the stage of monocytic differentiation. Moreover, the expression levels of Myh1, Myh2, Myh4, and Myh7 in the DM7 + 6 group were higher than those in the other two groups, indicating that most of the myoblasts in the DM7 + 6 group were in the stage of multinucleated differentiation [25], which again verified that the differentiation degree of the DM7 + 6 group was higher.

At the same time, the angiogenic genes CD31, CD34, CD144, and vWF in HUVEC cells were detected (Figure 5I ~ K). Compared with the DM1 + 6 group, the DM7 + 6 group had higher expression of platelet endothelial cell adhesion molecule (CD31), hematopoietic stem cell marker (CD34), and VE-cadherin (CD144), indicating more mature vascularization. [26-28]

Discussion

Existing vascularized skeletal muscle methods can construct structures with vascularization and muscle tubes, but there are still problems such poor biomimetic degree. [4,17] We intervene in vascularization to increase the complexity and biomimetic degree of skeletal muscle tissue construction through 3D printing and 3D modeling to achieve the structure of vascularized skeletal muscle which regulated the vascularization and myotubes in both time and space.

3D printing is a state-of-the-art technology in that individual geometries can be built quickly and precisely according to different requirements. [15] Subsequentially, its printing accuracy is high which can ensure that the PDMS mold can adjust the size according to the width of the muscle bundle to ensure that the thickness of HFG is uniform. 3D bioprinting can pre-modulate of the arrangement of cells in the constructed muscle bundles showing a more pronounced orientation compared to unprinted structures. [16, 29] Therefore, it can arrange living cells with biomaterials to generate specified three-dimensional structures by jetting or extrusion, creating tissues with intact structures that can be transplanted *in vitro*. [15] We selected gelatin and fibrinogen as printing inks to suit the requirements of mechanical properties, rheological properties, biological activity, and biocompatibility. [30-35]

The vascular network wrapped around the muscle bundle has a topology that is like the physiological structure and is more biomimetic. Compared with the naturally occurring arrangement of adipocytes (fat cells) and blood vessels within macroscopic skeletal muscle, and the design of arterioles and venules accompanying muscle fascicles, the arterial and venous networks, when constructed separately, cannot adequately perfuse a 5 mm wide muscular structure due to limitations in nutrient supply capacity. [13, 36] However, our goal is to engineer a highly organized vascular network that mirrors the dense capillary beds found in terminal arterioles, venules, and microvascular units, to achieve sufficient nutrient delivery throughout the entire muscle tissue. Additionally, the culture method of extra vascularizing HFG in the differentiation process can realize the time regulation of vascularization and the selection of the time point of co-culture between blood vessels and myotubes. This methodology can be utilized as a tissue model to investigate the relationships between myotubes and vascularization.

In vascularized skeletal muscle tissue, C2C12 and HUVEC have different requirements for differentiation conditions [37] It is impossible to coordinate the differentiation conditions between the two types of cells during co-culture that can create a structure with mature vascularization and myotubes when regulated the onset time of vascularization. By comparing the expression of the vascularization marker CD31 with the myotubulization marker MHC and molecular level, it is more conducive to forming a more mature myotube structure after seven days of differentiation. [24] Higher vascularization marker gene expression can be observed at the molecular level when the vascular network is initiated later. In summary, when the vascular network is created, an EGM2 medium must be added to maintain the survival and differentiation of HUVECs and keep the cells maintaining in a high-proliferation environment.

However, the medium used for C2C12 differentiation is 2% HS (DMEM), a differentiation environment devoid of proliferative factors, which inhibits the differentiation of C2C12 and significantly slows down the process of myotubes formation. [8] We discovered that after C2C12 differentiation to form myotubes and then starting vascularization of the myotubes formed by differentiation, the myotubes formed by differentiation will maintain the current state.

We artificially regulate the construction of vascular networks at different stages of fascicular differentiation to regulate the co-culture initiation time and differentiation process of the two types of cells. The vascular network starts when the fascicle is in the mononuclear differentiation period, resulting in the C2C12 always maintaining a low differentiation level in the muscle bundle. However, when C2C12 was in the early stage of multinuclear differentiation, the vascular network was established, and obvious multinuclear myotubes appeared inside the muscle bundle, although the maturity was subpar. Simultaneously, when C2C12 was in the middle and late stages of multinuclear differentiation, the vascular network began to be constructed, and it could be seen that there would be mature myotubes and a more evident vascular network (Fig 6). Therefore, initiating vascular network construction after the formation of secondary myotubes is a way to promote the construction of *in vitro* vascularized skeletal muscle that maximizes the maturity of the internal structure of the tissue.

Conclusion

In this study, we constructed skeletal muscle using 3D bioprinting technology, complemented by the creation of a vascular network through 3D modeling technology. By modulating the interaction modes and timing between endothelial cells and muscle cells, and employing techniques such as immunofluorescence staining and RT-qPCR detection, we have found that establishing the vascular network during the later stages of muscle bundle differentiation is beneficial for the formation of muscle tubes. This method, involving the regulated introduction of medium and sequential cell insertion, proves more effective for the co-culture of endothelial cells and myoblasts in our system. It also opens avenues for further exploration of the interplay between muscle bundle development and vascularization. However, it is noteworthy that the vascularized outer layer does not yet fully penetrate the inner skeletal muscle tissue to provide oxygen and nutrients, highlighting the ongoing challenges in fabricating bionic multicellular tissues.

Acknowledgments

The authors acknowledge funding support from the National Natural Science Foundation of China (T2222029, U21A20396, and 62127811), the Strategic Priority Research Program of the Chinese Academy of Sciences (XDA16020802), and the CAS Project for Young Scientists in Basic Research (YSBR-012), and imaging technical support from Shiwen Li, Guoli Hou, and Xili Zhu of the CAS Imaging Platform.

Author contributions

Qi Gu designed the experiments, supervised the work, and revised the manuscript. Minxuan Jia, Tingting Fan, and Tan Jia performed the experiments and analysed the results. Minxuan Jia wrote and revised the manuscript. Xin Liu and Heng Liu discussed the results and prepared the manuscript.

Conflict of Interests

The authors declare no conflict of interest.

Supporting Information

Supplementary material is shown in an additional file.

Reference

1. W. R. Frontera, J. Ochala (2015) Skeletal muscle: a brief review of structure and function. Tissue Int 96 (3): 183-95.

http:// doi: 10.1007/s00223-014-9915-y.

2. A. R. Gillies, R. L. Lieber (2011) Structure and function of the skeletal muscle extracellular matrix. Muscle Nerve 44(3): 318-31. http:// doi: 10.1002/mus. 22094.

3. D. Dziedzic, U. Bogacka, B. Ciszek (2014) Anatomy of sartorius muscle. Folia Morphol 73(3): 359-62. http: // doi: 10.5603/fm. 2014. 0037

4. I. M. Olfert, O. Baum, Y. Hellsten, S. Egginton (2016) Advances and challenges in skeletal muscle angiogenesis. Am J Physiol-heart C 310(3): H326-36. http:// DOI: 10.1152/ajpheart. 00635. 2015

5. D. Gholobova, L. Terrie, M. Gerard, H. Declercq, L. Thorrez (2020) Vascularization of tissue-engineered skeletal muscle constructs. Biomaterials 2020. 235: 119708. http:// DOI: 10. 1016/j. biomaterials. 2019. 119708

6. D. N. Granger, E. Senchenkova (2010) Colloquium series on integrated systems physiology: from molecule to function. Inflammation and the Microcirculation 2010. 2(1): 1-87. http:// doi: 10. 1002/adhm. 201900626

7. A. Moriscot, E. H. Miyabara, B. Langeani, A. Belli, S. Egginton, T. S. Bowen (2021) Firearms-related skeletal muscle trauma: pathophysiology and novel approaches for regeneration. NPJ REGEN MED 6 (1), 17. http:// DOI: 10. 1038/s41536-021-00127-1

8. T. Osaki, V. Sivathanu, R. D. Kamm (2018) Crosstalk between developing vasculature and optogenetically engineered skeletal muscle improves muscle contraction and angiogenesis. Biomaterials 156: 65-76 http:// DOI: 10.1016/j. biomaterials. 2017. 11. 041

9. B. T. Corona, J. C. Rivera, J. G. Owens, J. C. Wenke, C. R. Rathbone (2015) Volumetric muscle loss leads to permanent disability following extremity trauma. J Rehabil Res Dev 52(7): 785-792. http:// DOI: 10.1682 / JRRD. 2014. 07. 0165

10. M. Stevanovic, F. Sharpe (2014) Functional free muscle transfer for upper extremity reconstruction. Plast Reconstr Surg 134(2):257e-274e. http:// DOI: 10.1016 / j. cps. 2011. 09. 001

11. P. Zhuang, J. An, C. K. Chua, L. P. Tan (2020) Bioprinting of 3D in vitro skeletal muscle models: A review. Materials & Design 193. http:// DOI: 10. 1186 / s13567-021-00942-w

12. Y. J. Choi, Y. J. Jun, D. Y. Kim, H. G. Yi, S. H. Chae, J. Kang, J. Lee, G. Gao, J. S. Kong, J. Jang, W. K. Chung, J. W. Rhie, D. W. Cho (2019) A 3D cell printed muscle construct with tissue-derived bioink for the treatment of volumetric muscle loss. Biomaterials. 206: 160-169. http:// DOI: 10. 1016/j. biomaterials. 2019. 03. 036

13. Gilbert-Honick, W. Grayson (2020) Vascularized and Innervated Skeletal Muscle Tissue Engineering. Adv Healthc Mater. 2020, 9 (1), e1900626. http:// DOI: 10. 1002/adhm. 201900626

14. M. Beldjilali-Labro, A. Garcia Garcia, F. Farhat, F. Bedoui, J. F. Grosset, M. Dufresne, C. Legallais (2018) Biomaterials in Tendon and Skeletal Muscle Tissue Engineering: Current Trends and Challenges. Materials 11 (7). http:// DOI: 10.3390/ma 11071116

15. H. W. Kang, S. J. Lee, I. K. Ko, C. Kengla, J. J. Yoo, A. Atala (2016) A 3D bioprinting system to produce human-scale tissue constructs with structural integrity. Nat. Biotechnol 34 (3), 312-9. http:// DOI: 10. 1038/nbt. 3413

16. T. Fan, S. Wang, Z. Jiang, S. Ji, W. Cao, W. Liu, Y. Ji, Y. Li, N. Shyh-Chang, Q. Gu (2021) Controllable assembly of skeletal muscle-like bundles through 3D bioprinting. Biofabrication 14 (1). http:// DOI: 10. 1088 / 1758-5090/ac3aca

17. S. R. I. Jordana Gilbert-Honick, Sarah M. Somers, Richard M. Lovering Kathryn Wagner, Hai-Quan Mao, Warren L. Grayson (2018) Engineering functional and histological regeneration of vascularized skeletal muscle. Biomaterials 164: 70-79. http:// DOI: 10.1016 / j. biomaterials. 2018. 02. 006

18. L. Pinton, M. Khedr, V. M. Lionello, S. Sarcar, S. M. Maffioletti, S. Dastidar, E. Negroni, S. Choi, N. Khokhar, A. Bigot, J. R. Counsell, A. S. Bernardo, P. S. Zammit, F. S. Tedesco (2023) 3D human induced pluripotent stem cell-derived bioengineered skeletal muscles for tissue, disease and therapy modeling. Nat Protoc. 18(4): 1337-1376. http:// doi: 10. 1038/s41596-022-00790-8

19. M. R. Garcia-Cruz, A. Postma, J. E. Frith, L. Meagher, (2021) Printability and bio-functionality of a shear thinning methacrylated xanthan-gelatin composite bioink. Biofabrication. 2021, 13 (3). http:// DOI: 10. 1088/1758-5090/abec2d

20. M. W. Laschke, Y. Harder, M. Amon, I. Martin, J. Farhadi, A. Ring, N. Torio-Padron, R. Schramm, M. Rücker, D. Junker, J. M. Häufel, C. Carvalho, M. Heberer, G. Germann, B. Vollmar, M. D. Menger (2006) Angiogenesis in tissue engineering: breathing life into constructed tissue substitutes. Tissue Eng 12(8): 2093-2104. http:// DOI: 10. 1089/ten. 2006. 12. 2093

21. I. Miranda, A. Souza, P. Sousa, J. Ribeiro, E. M. S.

Castanheira, R. Lima, G. Minas (2021) Properties and Applications of PDMS for Biomedical Engineering: A Review. JFB. 2021, 13 (1). http:// DOI: 10. 3390 / jfb13010002

22. A. Gokaltun, M. L. Yarmush, A. Asatekin, O. B. Usta (2017) Recent advances in nonbiofouling PDMS surface modification strategies applicable to microfluidic technology. Technology. 5(01): 1-12. http:// DOI: 10. 1142 / S2339547817300013

23. M. Schmidt, S. C. Schuler, S. S. Huttner, B. von Eyss, J. von Maltzahn (2019) Adult stem cells at work: regenerating skeletal muscle. Cell Mol Life Sci. 76(13): 2559-2570. http:// DOI: 10.1007/s00018-019-03093-6

24. S. Bersini, I. K. Yazdi, G. Talo, S. R. Shin, M. Moretti, A. Khademhosseini (2016) Cell-microenvironment interactions and architectures in microvascular systems. Biotechnol Adv. 34(6): 1113-1130. http:// DOI: 10. 1016 / j. biotechadv. 2016. 07. 002

25. J. Chal, O. Pourquie (2017) Making muscle: skeletal myogenesis in vivo and in vitro. Development. 144(12): 2104-2122. http:// DOI: 10. 1242/dev. 151035

26. E. Dejana, F. Orsenigo (2013) Endothelial adherens junctions at a glance. J Cell Sci. 126: p. 2545-2549. http:// DOI: 10.1242/jcs. 124529

27. L. E. Sidney, M. J. Branch, S. E. Dunphy, H. S. Dua, A. Hopkinson (2014) Concise review: evidence for CD34 as a standard marker for diverse progenitors. Stem Cells. 32(6): 1380-1389. http:// DOI: 10.1002/stem.1661

28. P. Lertkiatmongkol, D. Liao, H. Mei, Y. Hu, P. J. Newman (2016) Endothelial functions of platelet/endothelial cell adhesion molecule-1 (CD31). Curr Opin Hematol. 23(3): 253-259. http:// DOI: 10. 1097 / MOH.0000000000000239

29. J. H. Kim, Y. J. Seol, I. K. Ko, H. W. Kang, Y. K. Lee, J. J. Yoo, A. Atala, S. J. Lee (2018) 3D Bioprinted Human Skeletal Muscle Constructs for Muscle Function Restoration Scientific Reports. http:// DOI: 8 (1), 12307. 10.1038/s41598-018-29968-5.

30. T. Distler, A. A. Solisito, D. Schneidereit, O. Friedrich, R. Detsch, A. R. Boccaccini (2020) 3D printed oxidized alginate-gelatin bioink guides C2C12 muscle precursor cell orientation and differentiation via shear stress during bioprinting. Biofabrication. 12 (4), 045005. http:// DOI: 10. 1088/1758-5090/ab98e4

31. B. Kaczmarek, K. Nadolna, A. Owczarek (2020) The physical and chemical properties of hydrogels based on natural polymers. J Mater Sci Mater Med 12(4): 045005. http:// DOI: 10. 1007/s10856-019-6318-7

32. D. B. Kolesky, R. L. Truby, A. S. Gladman, T. A. Busbee, K. A. Homan, J. A. Lewis (2014) 3D bioprinting of vascularized, heterogeneous cell-laden tissue constructs. Adv Mater. 2014, 26(19): 3124-30. http:// DOI: 10. 1016 / j. actbio. 2018. 02. 007

33. J. Yu, K. Wang, C. Fan, X. Zhao, J. Gao, W. Jing, X. Zhang, J. Li, Y. Li, J. Yang, W. Liu (2021) An Ultrasoft Self-Fused Supramolecular Polymer Hydrogel for Completely Preventing Postoperative Tissue Adhesion. Adv Mater. 33 (16), e2008395. http:// DOI: 10. 1002 / adma. 202008395

34. J. Saroia, W. Yanen, Q. Wei, K. Zhang, T. Lu, B. Zhang (2018) A review on biocompatibility nature of hydrogels with 3D printing techniques, tissue engineering application and its future prospective. BDM 1: p. 265-279. https://doi. org/10.1007/s42242-018-0029-7

35. M. Dietrich, J. Heselhaus, J. Wozniak, S. Weinandy, P. Mela, B. Tschoeke, T. Schmitz-Rode, S. Jockenhoevel (2013) Fibrin-based tissue engineering: comparison of different methods of autologous fibrinogen isolation. Tissue Eng Part A. 19(3): 216-226. http:// DOI: 10.1089 / ten. TEC. 2011. 0473

36. D.-H. Kang, F. Louis, H. Liu, H. Shimoda, Y. Nishiyama, H. Nozawa, M. Kakitani, D. Takagi, D. Kasa, E. Nagamori, S. Irie, S. Kitano,M. Matsusaki (2021) Engineered whole cut meat-like tissue by the assembly of cell fibers using tendon-gel integrated bioprinting. Nat Commun https://doi.org/10.1038/s41467-021-25236-9

37. R. K. Jain, P. Au, J. Tam, D. G. Duda, D. Fukumura (2005) Engineering vascularized tissue. Nat. Biotechnol. 2005, 23 (7), 821-3. http:// doi: 0.1038/nbt070